Icarus 221 (2012) 710–720

Contents lists available at SciVerse ScienceDirect

Icarus

journal homepage: www.elsevier.com/locate/icarus

Layered MegaBlocks in the central uplifts of impact craters

C.M. Caudill [a,*], L.L. Tornabene [b], A.S. McEwen [a], S. Byrne [a], L. Ojha [a], S. Mattson [a]

[a] University of Arizona, Lunar and Planetary Laboratory, 1541 E University Blvd., Tucson, AZ 85721, United States
[b] University of Western Ontario, Centre for Planetary Science and Exploration (CPSX), 1151 Richmond Street, London, ON, Canada N6A 5B7

ARTICLE INFO

Article history:
Received 6 February 2012
Revised 25 August 2012
Accepted 29 August 2012
Available online 14 September 2012

Keywords:
Mars
Cratering
Volcanism

ABSTRACT

A database of bedrock exposed in crater central uplifts has been compiled from multiple orbital datasets. In this study we focus on uplifts which show decameter-scale layers within the exposed megablocks derived from the bedrock of the preexisting target. This distinctive morphology, found in 41 craters globally, occurs mostly in regions mapped as Hesperian plains material, generally interpreted as regions of extensive flood lavas. The association with volcanic units coupled with morphology and mineralogy that is consistent with flood lava emplacement suggests that the layers are stacks of dense lava interbedded with weaker materials. Estimates for the uplift of stratigraphic sections coupled with morphologic and morphometric analyses lead to estimated thicknesses of the layered unit. These estimates indicate Hesperian flood lavas are ~23% thicker than a previous minimum estimate, with a volume of 5.5×10^7 km^3. This increases the known extrusive volcanic production for the history of Mars and volatile release to past martian atmospheres.

1. Introduction

Impact craters are abundant on Mars and expose the shallow subsurface in their walls. Large, complex craters expose deeper bedrock during late-stage crater formation expressed in central uplift features. The subsurface geology of a planetary body is difficult to study from remote-sensing data, however bedrock uplifted in these central features allows such an undertaking (e.g., Tompkins and Pieters, 1999). Such study is vital to understanding planetary history and geologic processes. Study of exposures in deep canyons such as Valles Marineris (e.g., Geissler et al., 1990; McEwen et al., 1999; Beyer and McEwen, 2005; Flahaut et al., 2010) provide subsurface information, but large regions of Mars lack such canyons. Also, foreshortening hampers the observation of bedrock from above in steep canyon walls (especially nearly horizontal layered bedrock). Observations made by the High Resolution Imaging Science Experiment (HiRISE; McEwen et al., 2007, 2010) aboard the Mars Reconnaissance Orbiter (MRO) have revealed crater central features (peaks, floor pits and summit or peak pits) having exhumed massive (m-km scale), relatively intact blocks of the pre-impact target bedrock. Exploiting martian impact crater formation (which expose subsurface materials) and preservation of their central feature morphology (except where covered by regolith or aeolian deposits) allows a unique opportunity to explore the underlying stratigraphy and geologic history of Mars. This study builds on a survey of these craters (Crater Exposed Bedrock database, Tornabene et al., 2010) in over 900 HiRISE observations, which yielded specific bedrock classifications. Thermal Emission Imaging System (THEMIS, Christensen et al., 2004) nighttime thermal infrared images were used as a first order assessment of thermophysical properties, which indicates where bedrock may exist (e.g., Edwards et al., 2009). Hence, the survey includes all equatorial and mid-latitude regions while omitting areas or craters with thermophysical properties indicative of poor bedrock exposure. This includes high-latitude polar regions, ranging in latitude from 70S to 80N, and areas of dense dust or surface cover (e.g., Arabia Terra). Craters with thermophysical properties indicative of potential bedrock exposure were followed up with analysis of HiRISE high-resolution images, which resulted in sample population distribution shown in Fig. 1. Some of these craters actually lack good bedrock exposures (rocky regolith gives the same thermophysical signature as areas with partial bedrock exposure) and were not analyzed further.

In this study, we focus on Layered MegaBlock (LMB) bedrock exposures. LMB is defined as a central uplift comprised of large megablocks (100s to 1000s of meters in diameter) of the preexisting target that was uplifted and tilted by the impact process. The megablocks specifically consist of layered rock, with the individual layer thicknesses ranging from meter to decameter scales (Fig. 2). LMB are examined here to discern its origin by using specific datasets, morphologic and lithologic analogs, and morphometric analysis. The HiRISE dataset in particular allows for analysis of meter-scale

* Corresponding author. Fax: +1 520 770 3505.
E-mail addresses: caudill@email.arizona.edu (C.M. Caudill), ltornabe@uwo.ca (L.L. Tornabene), mcewen@lpl.arizona.edu (A.S. McEwen), shane@lpl.arizona.edu (S. Byrne), luju@email.arizona.edu (L. Ojha), smattson@pirl.lpl.arizona.edu (S. Mattson).

0019-1035/$ - see front matter © 2012 Elsevier Inc. All rights reserved.
http://dx.doi.org/10.1016/j.icarus.2012.08.033

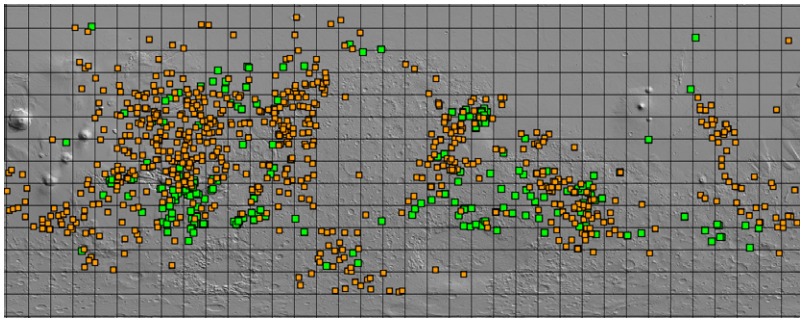

Fig. 1. Distribution of 919 craters surveyed, overlain onto MOLA shaded relief map. Green points indicate bedrock exposures with small-scale features identified with HiRISE images. Orange points indicate analyzed craters having no clear evidence of significant bedrock exposure. Latitude range 70S–70N, Simple Cylindrical map projection. (For interpretation of the references to color in this figure legend, the reader is referred to the web version of this article.)

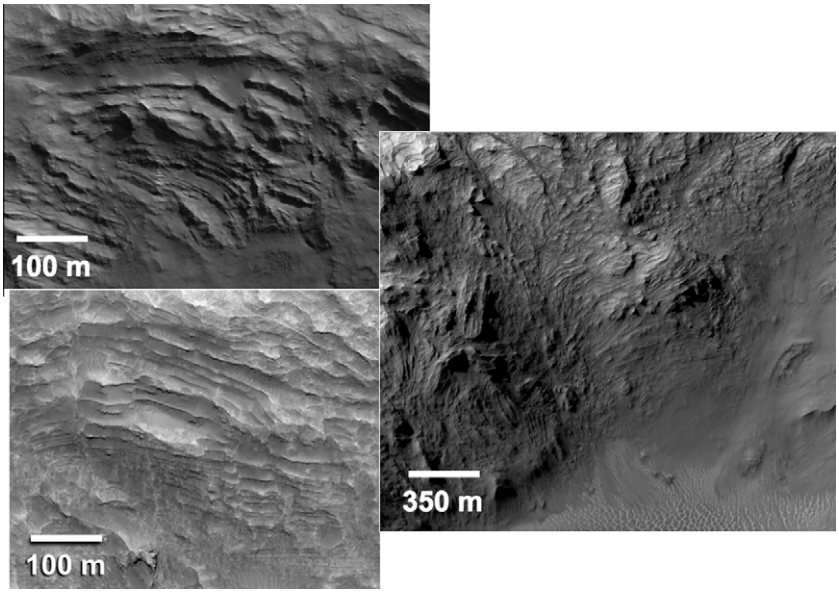

Fig. 2. (Top left) Central uplift of crater in Bosphorus Planum, seen in HiRISE image ESP_018703_1570. Image rotated, Sun from top of image and phase angle 62°. (Bottom left) Central peak pit structure of an unnamed crater in Thaumasia Planum, seen in HiRISE image PSP_005201_1640. Image rotated, Sun from top of image and phase angle 39°. (Right) Central peak pit structure of Mazamba Crater, HiRISE image PSP_007100_1520. Sun from north (top of image), phase angle 55°.

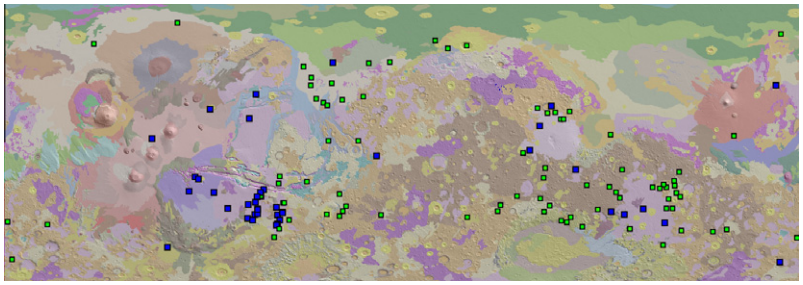

Fig. 3. Distribution of bedrock identified in crater central uplifts overlain onto a geologic map (Skinner et al., 2006); Purple units are Hesperian ridged plains and pink units are Amazonian volcanics. Blue points represent layered bedrock (~90% correlation with Hesperian ridged plains) and green points represent additional bedrock textures without layered material (~40% correlation with Hesperian ridged plains). Latitude range −50N to 60N, Simple Cylindrical map projection. (For interpretation of the references to color in this figure legend, the reader is referred to the web version of this article.)

morphology and morphometric data collection, where resolution of layering is necessary to assess individual layer thickness and erosional characteristics. Coupled with crater scaling techniques and the regional geologic context, we use these observations to estimate the source depths of LMB material and, by extension, constrain a total volume. The regional geologic context for LMB is seen by overlaying the survey data points of bedrock outcroppings on a geologic map; Fig. 3 shows LMB bedrock outcroppings represented by blue points. Other identified bedrock textures from the survey, which do not have LMB outcroppings, are shown in green.

2. Background

2.1. Central uplift formation

Martian impact craters with final rim diameters greater than ~5–7 km exhibit modification resulting in a complex morphology consisting of terraced walls, lower depth-to-diameter relationships than simple craters, and a central feature (Pike, 1980; Garvin and Frawley, 1998). Impact formation is conventionally broken down into three main stages, beginning with the projectile penetrating the surface and producing intense shock waves that propagate through the target material. This projectile is transformed into melt and vapor (e.g., Melosh, 1989). The second stage excavates the target material creating a bowl-shaped transient cavity. Impact melt and breccias line the transient cavity floor, which consists of fractured and displaced target rock (e.g., French, 1998). During the last stage of modification, the fundamental strength of the sub-crater floor rock is affected by the attenuating shock waves that cause the rock to be excavated and uplifted from depth. This depth from which the target bedrock material originates is known as stratigraphic section uplift (called "section uplift" or SU hereafter), and results in a central peak feature of folded, faulted, and rotated megablocks (Pilkington and Grieve, 1992; Grieve and Therriault, 2004). The original depth of this exhumed bedrock has been estimated for terrestrial structures as approximately 1/10 the final crater rim diameter (Grieve et al., 1981; Pilkington and Grieve, 1992). This study uses a later refinement of this model by Grieve and Pilkington (1996), which considered a greater number of terrestrial impact structures. Variations in impactor type (Cintala and Grieve, 1993) or gravitational variations between the Moon, Earth, and Mars are not thought to be significant factors in how SU varies with diameter (O'Keefe and Ahrens, 1999). However, the terrestrial-based SU equation may not be highly accurate because the craters are often deeply eroded or buried and their original diameters are difficult to estimate (Melosh, 1989).

General types of uplift structures include central peaks and central pits. Central pits can be further subdivided into floor pits, where only a topographic depression in the crater floor remains, and peak or summit pits, which have a depression at the summit of an uplifted peak or ring of hills (Grieve et al., 1981). The formation mechanisms of these central pits are not well known, but have been suggested to form as a result of subsurface volatile degassing by Wood et al. (1978) or drainage of impact melt into sub-crater fractures and not likely due to central peak gravity collapse (Bray et al., 2012). Central pits have been found to be more common on units mapped and interpreted as lava rather than sedimentary targets, which suggests that the target material may play a role in determining in central uplift morphology (Whitehead et al., 2010). However, we note that craters into lava plains are also better preserved than those into martian sediments, which are easily eroded.

2.2. Basic morphology of LMB

The individual layers of LMB have a distinct morphology, where darker-toned layers alternate with shallower or lower-standing light-toned layers. Often, lower-standing layers are visually obscured by overlying dust or aeolian deposits, and are thus more difficult to analyze morphologically. The unique appearance of LMB is shown in Fig. 4 (right), where the light-toned alternate layers are exposed and can be seen in detail as fractured material. The fracturing may have occurred during crater formation. Central uplifts and neighboring fracture zones of terrestrial and martian craters are known to experience hydrothermal circulation consequent of the impact event (Komor et al., 1988; Larson et al., 2009). Stresses undergone by a section as it is thrust to the surface may also leave km-scale folds and faults throughout the central uplift (Fig. 4, left).

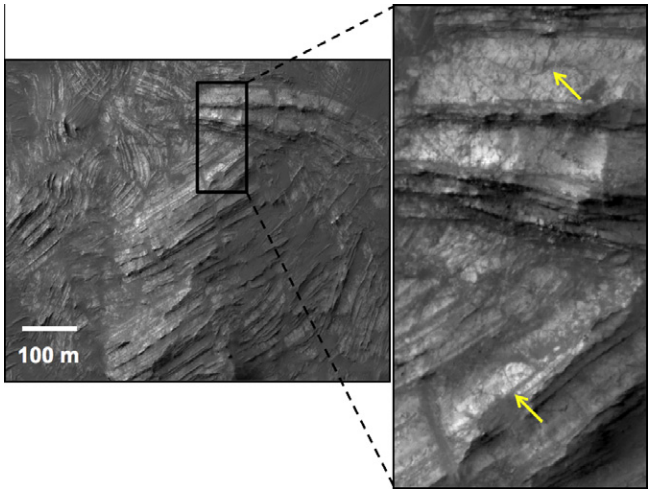

Fig. 4. Unnamed crater central peak in Solis Planum, HiRISE ID ESP_016805_1565, with light-toned layered material throughout LMB outcropping (left), and darker overlying loose aeolian material. Image is zoomed in (right) to show texture; the light-toned lower-standing layers show fractures (yellow arrows). (For interpretation of the references to color in this figure legend, the reader is referred to the web version of this article.)

2.3. Geologic setting for LMB craters

Mars has been mapped into three main time-stratigraphic units: Noachian (older than ~3.9 Gy), Hesperian (~3.9–3.0 Gy), and Amazonian (~3 Gy to present) (Tanaka, 1986). The Hesperian epoch is characterized geologically by slowed rates of impact events, weathering, and erosion compared to the Noachian, and high average rates of volcanic activity (which drops off by a factor of 10 during the Amazonian age) (Carr and Head, 2010). Hesperian-aged ridged plains have been mapped over extensive regions of Mars and have been interpreted to be volcanic flood lavas (Scott and Tanaka, 1986; Greeley and Guest, 1987; Keszthelyi and McEwen, 2007). Hesperian plains units were defined by Scott and Tanaka (1986) and Greeley and Guest (1987) using surface morphology to map homogenous stratigraphic units and measuring crater densities to infer their relative ages. Distinctive Hesperian-aged plains surface morphology known as wrinkle-ridges are commonly accepted to form when contractional deformation differentially affects underlying and surface stratigraphy having differing layer strengths, as when a stronger lava layer overlies weaker sediments (Golombek et al., 2001). This is analogous to terrestrial Large Igneous Provinces, where sequence stratigraphy of lava flows with intervening sediment or soil layers are known as cooling units (Nichols, 1936; Self et al., 1997). These packages of stratigraphy imply temporal separation in emplacement and subsequent cooling of outpourings of lava. Hesperian ridged plains are interpreted as broad, thin lava flows (Greeley and Spudis, 1981) much like terrestrial Large Igneous Provinces. Although martian lava flows differ from terrestrial flows due to generally higher eruption rates and lower gravity (Wilson and Head, 1994), terrestrial Large Igneous Provinces still serve as useful analogs for large-scale effusive volcanism on Mars. Volume estimates of terrestrial Large Igneous Provinces are difficult to estimate due to tectonism, erosion, and/or burial processes (Bryan et al., 2010), but estimates are based on areal extent multiplied by depth estimates both terrestrially and on Mars (Ernst et al., 2004). The total volume of the Columbia River Flood Basalt Group (northwestern US) unit is estimated to be ~234,000 km^3 (Hales et al., 2005), with episodic

emplacement covering areas of up to 200,000 km^2 (Riedel, 2005) and building a thick stratigraphic unit over a time span of ~1 Myr. Comparatively, the best-preserved martian flood lava in Elysium Planitia has an estimated 250,000 km^2 of coverage with less certain total volumes (Jaeger et al., 2010).

In this study, we used the Java Mission-planning and Analysis for Remote Sensing GIS software package (JMARS; Christensen et al., 2009). A shapefile subset of the Crater Exposed Bedrock database (Tornabene et al., 2010) containing the 41 crater central uplifts expressing LMB texture was overlain on a geologic map (Skinner et al., 2006), shown in Fig. 3. LMB outcroppings are strongly correlated with mapped Hesperian plains material. 90% of LMB outcroppings fall in Hesperian volcanic plains units (~73% fall in Hesperian ridged plains, ~17% fall in Hesperian Syrtis Major and Hesperian Syria Planum Formations). Other identified bedrock textures from the survey, shown in green, do not have LMB outcroppings and do not correlate well with mapped volcanic plains; ~40% of the non-LMB bedrock outcroppings were found in these areas.

Valles Marineris is the largest and deepest direct exposure of layered rock on Mars. It occurs in regions mapped as Hesperian ridged plains (as well as Hesperian Syria Planum Formation) and in close proximity of many LMB outcroppings in this study. The meters- to decameters-thick layers concentrated in the upper parts of Valles Marineris are interpreted as flood lavas interspersed with sediments such as pyroclastics and perhaps intrusives (McEwen et al., 1999; Schultz, 2002; Williams et al., 2003; Beyer and McEwen, 2005; Keszthelyi and McEwen, 2007). Malin and Edgett (2001) questioned this interpretation from Mars Orbital Camera (MOC) observations, in part because "... there are few boulders at the bottoms of the walls of Valles Marineris. This observation suggests that the boulders derived from layered materials do not have sufficient strength to survive descent ..." However, Beyer and McEwen (2005) noted that many large blocks (>3 m) could be seen by MOC in landslide deposits derived from the upper layers, and HiRISE images show great numbers of boulders that are smaller than 3 m diameter. In addition, the higher resolution HiRISE images of the layers (Keszthelyi et al., 2008) support the volcanic interpretation as well as the recent discovery of mafic to ultramafic dikes and outcrops deep in Valles Marineris (Edwards et al., 2008; Flahaut et al., 2011). It is noted by Flahaut et al. (2012) that the morphology and non-detection of sulfates or fine sedimentary layers within the wall bedrock of Valles Marineris (rather than pasted on the outside) is consistent with repeated Noachian and Hesperian basaltic volcanics, supporting the results of Edwards et al. (2008). The large cluster of LMB craters found south of Valles Marineris allows us to compare the material exhumed from depth by the central uplift of these craters to the layered material exposed in the canyon system. Flahaut et al. (2012) also made a similar comparison, noting that the western regions of Valles Marineris contain dark layers consistent with layers exposed within a few central uplifts of craters in the region.

3. Data, methods, and analysis

3.1. Morphometry

Bedrock exposures in well-preserved crater central uplifts were targeted by HiRISE after surveying them with Mars Orbiter Laser Altimeter (MOLA; Smith et al., 2001) and THEMIS nighttime infrared datasets. Those exposures that are relatively bright or warm at night (consistent with high thermal inertia) were considered likely to exhibit bedrock exposures with the least obscuration by dust or other fine-grained surface deposits. Context Camera (CTX; Malin et al., 2007) data was also used to preliminarily identify bedrock exposures, but only HiRISE (25–50 cm/pixel) data can resolve the small-scale features of the outcrops that allow for specific identification of bedrock type (see Tornabene et al., 2010). LMB outcrops identified in HiRISE stereo pairs were analyzed using with SOCET SET (©BAE Systems, Inc.) digital photogrammetry software. Layered and stratified rocks on Mars are usually not oriented at a high enough tilt to easily infer their geometries from orbital imaging, however, the LMB layers are uplifted and rotated to orientations as to be useful for such determinations as strike, dip, and layer thickness. Exposed layers were mapped in 3D in SOCET SET for nine LMB outcroppings for which HiRISE stereo pairs were available for this study. These data were used to derive true bedding thickness and orientations by mapping any two adjacent layers, each defined by a 3D array of data points outlining the layer exposure. A best-fit plane in 3D space was fit to the mapped layers using the method of Byrne and Ivanov (2004). Layer thickness was calculated by finding the shortest distance between these two planes (which were generally not exactly parallel) at the location of the outcrop. Many layers are examined in each crater and these layer thicknesses are averaged for that specific central uplift (Table 1). Layer thickness averages were found to range from 2.8 m to 38.4 m.

Layers within LMB outcroppings have a distinct morphology, where higher-standing layers (typically darker-toned) appear to alternate with relatively lower-standing layers (Fig. 5). The difference in the relative height of layers was measured to infer lithologic characteristics such as erosional susceptibility. HiRISE-derived Digital Terrain Models (DTMs) (1 m/post and ~20 cm vertical precision—Kirk et al., 2008) were used to measure relative layer height differences (i.e., adjacent layers). Elevation profiles were extracted from transects that were drawn perpendicular as possible to the apparent layers within LMBs, produced using the Environment for Visualizing Images (ENVI, ITT Visual Information Solutions) geospatial software. These elevation profiles were then displayed graphically, where a line was fitted to the higher-standing layers (Fig. 5, right, yellow non-vertical lines) while allowing for local topographic variations. The height difference was then derived by measuring the elevation difference between the lower-standing layers and the fit line. Martin Crater (−21°S, 290°E, D = 58.5 km, SU = 5.28 km) and an unnamed crater (D = 53.5 km, SU = 4.82 km) ~400 km NE of Martin Crater were found to have layer height differences of 7.39 m and 7.72 m, respectively. 5500 km to the southwest, an unnamed crater in Terra Cimmeria (−47°S, 171°E, D = 34 km, SU = 3.0 km) was found to have LMB with a very different elevation profile, where the average difference between the higher and lower-standing layers was found to be 1.63 m. These measurements do not convey layer orientation or layer thickness (as in Table 1), but are presented here to separate the two layer types that exist within LMB outcrops – one of which is inferred to be less susceptible to erosion (darker-toned layers as seen in Fig. 4) than the other (lighter-toned layers).

Table 1
Layer thicknesses measured from HiRISE stereo pairs.

HiRISE image IDs	Average layer thickness (m)	Average layer orientation (°)
ESP_024095_2230_PSP_007652_2230	19.58	27
ESP_018057_2085_ESP_017635_2085	16.44	18
ESP_017833_1975_ESP_017055_1975	10.37	21
ESP_013679_1515_PSP_003803_1515	2.86	25
ESP_018703_1570_ESP_019204_1570	38.35	18
ESP_019271_1640_ESP_018282_1640	6	27
PSP_003408_1585_PSP_002353_1585	36.74	20
ESP_018611_1565_ESP_019323_1565	17.84	13
ESP_017556_1650_ESP_018268_1650	13.93	15

3.2. Crater scaling and section uplift

Our JMARS global database was overlain onto a global martian geologic map (Skinner et al., 2006) to examine the possible congruence of mapped surface materials and minimum age of exhumed bedrock type. A crater scaling relationship for section uplift provides estimates of the depths from which LMBs originate. We use the expression by Grieve and Pilkington (1996):

$$SU = 0.086D^{1.03}$$

(where D is the final crater rim diameter in kilometers) to estimate the maximum stratigraphic section uplift (SU). Using SU we assess the pre-impact stratigraphic positions of Crater Exposed Bedrock (Tornabene et al., 2010) outcroppings relative to each other. Syria, Sinai, Solis, Thaumasia, and Bosphorus Planums have 58% of the distribution of LMB craters found in this study, with final rim diameters ranging from 10.6 to 123.5 km. In Thaumasia Planum outcroppings are distributed throughout the Hesperian ridged plains unit, as seen in Fig. 6, including an unnamed crater 6.5 km south of Valles Marineris that has the smallest SU estimate in our study, 0.91 km. The range of these crater exposures extend to an estimated depth of 5.3 km locally. Bosphorus Planum craters have SU ranging from 1.1 to 3.3 km. Hesperia Planum, also mapped as Hesperian ridged plains, has only three observed LMB craters. The deepest exposure is 150 km from Tyrrhena Patera, near the center of Hesperia Planum. This unnamed crater (−23°S, 109°E) with 29.5 km diameter has an estimated SU of 2.6 km, the minimum SU of an LMB crater in this region (Table 2). The third observed cluster of LMB craters is in the Syrtis Major region, where four exposures span the regional Hesperian-aged plains. The minimum depth estimate of 2.79 km for the LMB material in this region is derived from an unnamed crater (−23°S, 68°E). Another unnamed crater ~825 km north of Nili Patera defines the maximum exposed depth of LMB material in this region, with a crater diameter of 66.3 km and a SU estimate of 6.01 km. Fig. 6 shows the section uplift estimates in our study.

3.3. Volume estimates

The sample population of LMB craters and their depth estimates provide some constraints on the subsurface extent and kilometer-scale thicknesses of the layered materials, as well as a means to estimate the volume of these materials. We need to estimate the original depth of the LMB relative to the pre-crater surface. MOLA-derived elevations are recorded for each LMB crater central feature (Table 2). Average surface elevation is then recorded based on MOLA ground points chosen on the surface near each crater, but outside of the uplifted rim and continuous ejecta blanket. To obtain estimates for the pre-impact thickness of layered bedrock represented by each crater, displayed in Table 2, the difference of the average surface elevation from the height of the central uplift feature is added to the estimate for SU (see schematic in Fig. 7). Regional volume estimates are then derived from the maximum estimated thickness of each region multiplied by the area of the region (Table 3). The area of the plains used in this study relies chiefly on geologic units mapped by Skinner et al. (2006) with additional surface morphology interpretations to define the unit

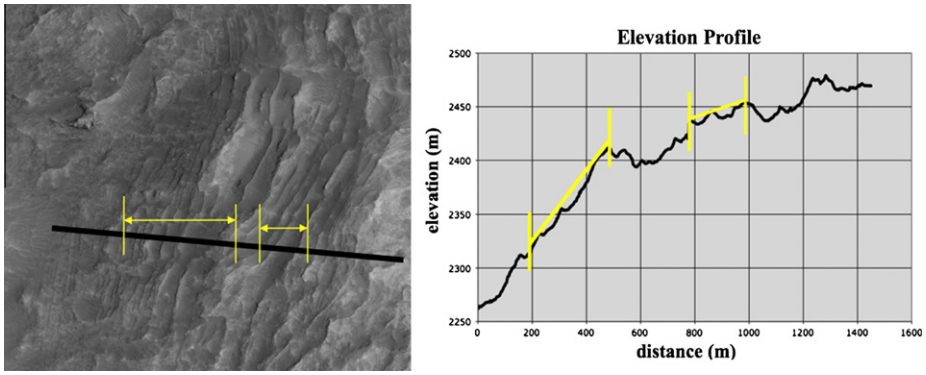

Fig. 5. (Left) Subset of HiRISE image PSP_005201_1640; LMB in peak pit of unnamed crater. Black line is a transect drawn across LMB unit. Yellow lines and arrows indicate two sections of layers used for measurements of alternating layer heights. (Right) Elevation profile of, again, the black transect (shown in the left image as well) taken from a HiRISE DTM of image. Yellow lines again show two sections of this unit used to measure alternating layer height, which are grouped based on a consistent slope within each section created by underlying topography. (For interpretation of the references to color in this figure legend, the reader is referred to the web version of this article.)

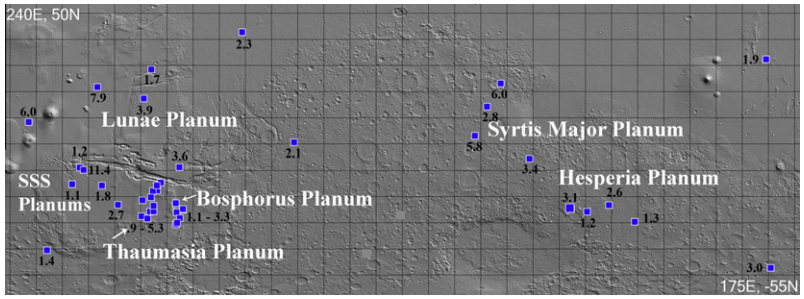

Fig. 6. LMB craters (blue points) with stratigraphic uplift estimates (SU, km) noted in black superimposed on a MOLA shaded relief map. Craters grouped in Thaumasia Planum and Bosphorus Planum have SUs displayed in a range due to the density of the LMB outcroppings in these regions. Thaumasia Planum contains 10 LMB with SU ranging from 0.9 to 5.3 km. Bosphorus Planum has seven tightly-grouped LMB with a SU range of 1.1–3.3 km. "SSS Planums" refers to Syria, Sinai, and Solis Planae. Latitude range −55N to 55N (Centric); Longitude range 175–240E; Simple Cylindrical map projection. (For interpretation of the references to color in this figure legend, the reader is referred to the web version of this article.)

Table 2
Summary of data locations, SU estimates, and MOLA-derived elevations for the LMB in central uplifts and elevations for the surrounding terrain. Craters are unnamed unless otherwise noted.

Region	Longitude (° East)	Latitude (° Centric)	HiRISE image ID	Crater diameter (km)	Section uplift (km)	Elevation central uplift (km)	Average surface elevation (km)	Estimated LMB unit thickness (km)
Acidalia Planitia	328.85	42.68	PSP_007652_2230	26	2.29	−5.41	−4.5036	3.20
Terrra Cimmeria	170.94	−47.29	ESP_021688_1325	34	3.01	1.013	1.975	3.98
Elysium Planitia	169.18	32.27	ESP_020290_2125	21.2	1.86	−4.205	−3.642	2.42
Hesperia Planum (Trinidad Crater)	109.06	−23.37	PSP_009427_1565	29.5	2.61	0.5205	1.625	3.71
Hesperia Planum	100.73	−25.8	ESP_018895_1540	14.3	1.24	0.50875	1.2373	1.97
Hesperia Planum	118.94	−29.72	PSP_006803_1500	15.4	1.34	0.489	1.26	2.11
Icaria Planum	254.18	−40.5	ESP_020485_1390	16.5	1.43	1.616	2.3536	2.17
Kasei Valles	294.01	28.39	ESP_017635_2085	19	1.66	−2.283	−1.5373	2.40
Lunae Planum	291.2	17.36	ESP_017055_1975	44.4	3.98	−1.256	−0.1543	5.08
Margaritifer Terra	348.73	0.61	ESP_020244_1805	24.4	2.15	−3.535	−2.0056	3.67
Bosphorus Planum	303.47	−30.69	ESP_019059_1490	14.4	1.25	0.482	1.0803	1.84
Bosphorus Planum	303.87	−26.01	ESP_017002_1535	31.3	2.77	−0.429	1.15	4.35
Bosphorus Planum	306.15	−25.04	ESP_017437_1550	12.8	1.1	0.488	0.98	1.60
Bosphorus Planum	306.17	−24.82	ESP_017437_1550	16.1	1.4	0.371	0.98	2.01
Bosphorus Planum	304.91	−28.37	ESP_013679_1515	18.7	1.63	0.3055	0.728	2.05
Bosphorus Planum	303.95	−30.02	ESP_018492_1495	15.4	1.34	0.348	0.9373	1.92
Bosphorus Planum	303.42	−22.59	ESP_018703_1570	36.7	3.27	0.6715	2.0313	4.63
Sinai Planum (Oudemans Crater)	268.24	−9.75	PSP_008340_1700	123.5	11.4	3.298	5.7823	13.89
Sinai Planum	275.24	−15.8	ESP_018282_1640	20.3	1.78	2.858	3.9155	2.83
Solis Planum	281.36	−23.16	ESP_016805_1565	31	2.75	1.14	2.4945	4.10
Syriai Planum	263.86	−15.3	ESP_019456_1645	12.7	1.1	5.4865	6.2008	1.81
Syrtis Major	67.66	23.06	PSP_012949_2030	66.3	6.01	−1.03	0.6183	7.66
Syrtis Major	62.48	14.14	PSP_010879_1945	31.5	2.79	0.433	1.2446	3.60
Syrtis Major (Leighton Crater)	57.77	3.1	PSP_007082_1830	64.5	5.84	0.49225	1.5883	6.94
Tharsis (Fesenkov Crater)	273.42	21.67	PSP_007931_2020	86.1	7.86	0.122	0.5816	8.32
Tharsis (Poynting Crater)	247.22	8.38	PSP_006930_1885	66.5	6.03	1.6555	2.9826	7.35
Thaumasia Planum	293.55	−25.76	PSP_008761_1540	27.5	2.43	1.5665	2.8506	3.71
Thaumasia Planum (Mazamba Crater)	290.34	−27.54	PSP_008036_1520	54.5	4.91	0.417	3.241	7.73
Thaumasia Planum	296.32	−17.68	PSP_008484_1620	51.5	4.63	1.223	3.3364	6.74
Thaumasia Planum	294.99	−25.71	ESP_018044_1540	12.2	1.05	2.2485	2.792	1.59
Thaumasia Planum	294.66	−17.89	ESP_015921_1620	20.5	1.79	3.067	3.6443	2.37
Thaumasia Planum	296.24	−15.87	PSP_005201_1640	53.5	4.82	2.234	3.805	6.39
Thaumasia Planum	293.98	−20.32	PSP_007469_1595	39.5	3.52	2.265	3.274	4.53
Thaumasia Planum (Martin Crater)	290.73	−21.42	PSP_002353_1585	58.5	5.28	2.21	3.216	6.29
Thaumasia Planum	292.55	−28.41	ESP_017398_1515	18.6	1.62	2.852	3.2716	2.04
Thaumasia Planum	294.88	−23.52	ESP_018611_1565	17.4	1.51	1.2415	2.8243	3.10
Tyrrhena Terra	78.66	−5.6	PSP_004365_1745	37.5	3.34	0.22275	1.2143	4.33
Tyrrhena Terra	94.51	−24.71	ESP_017603_1550	34.9	3.1	−0.7645	0.7606	4.63
Valles Marineris	266.68	−8.97	PSP_008841_1710	13.5	1.17	1.608	5.6716	5.23
Valles Marineris	297.67	−14.71	ESP_017556_1650	10.6	0.91	3.1	3.8176	1.63
Xanthe Terra (Elorza Crater)	304.76	−8.78	ESP_012479_1710	40.8	3.64	0.572	2.4153	5.49

areas. Fig. 3 shows Hesperian plains units, mapped as shades of purple, containing the majority of the LMB data points (~90%). Due to the constraints on the size, availability and position of LMB craters (i.e., randomly distributed and random diameters), the total volume of the layered material in the upper crust of these regions may be under-estimated. For example, the deepest LMB sampled by these craters is likely not the lowest (deepest) extent of the unit. Also, non-uniformity of the thicknesses of the underlying layered materials may be a cause for these volumes to be under- or over-estimates. Layered materials probably in-filled basins (deeper in the middle), so for example, a large crater near the edge may give an upper limit that is not representative.

4. Discussion

4.1. Relating LMB to Valles Marineris wall layering, volcanic scarps, and terrestrial flood basalts

We suggest that LMBs represent layered sequences of volcanic materials (lavas and pyroclastics, or reworked sediments derived from nearby volcanics), primarily emplaced during the late Noachian through Hesperian Epochs. 90% of LMB craters are found in units previously mapped as Hesperian-aged volcanic material (Fig. 3). Also, LMB layer strength and regional exposure depths (SUs) are consistent with what are interpreted to be exposed volcanic flood lava/sediment sequences in the walls of Valles Marineris (Beyer and McEwen, 2005). Note that while the uppermost layers may be Hesperian, the deeper layers could extend into the Noachian. Depth estimates based on LMB craters for Thaumasia and Bosphorus Planums (1.6–7.7 km) correlate to the depth of layered materials exposed in the walls of Ganges Chasma that are interpreted to be basaltic lava flows based on morphological and thermophysical properties (Craddock et al., 1997; Beyer and McEwen, 2005). CRISM analysis of several LMB craters south of Valles Marineris are consistent with mafic volcanics as interpreted by Quantin et al. (2011). They find dominant spectral absorption bands that indicate a mixture of olivine and high calcium pyroxene – typical of basalts. McEwen et al. (1999) observed that the wall layers of Valles Marineris consist of dark-toned bedrock alternating with shallower-sloped colluvium up to depths of 8 km that are morphological similar to the Columbia River Flood Basalt Group. Overall steep slopes of the outer wall of Valles Marineris have been found to result from layer strength consistent with terrestrial basaltic rock (Schultz, 2002), and the slopes appear to be supported primarily by the bedrock layers (Beyer and McEwen, 2005). Weaker intervening layers likely consist of some combination of tephra, regolith, aeolian deposits, fluvial sediments, and impact ejecta. Light-toned layered deposits inside Valles Marineris have been

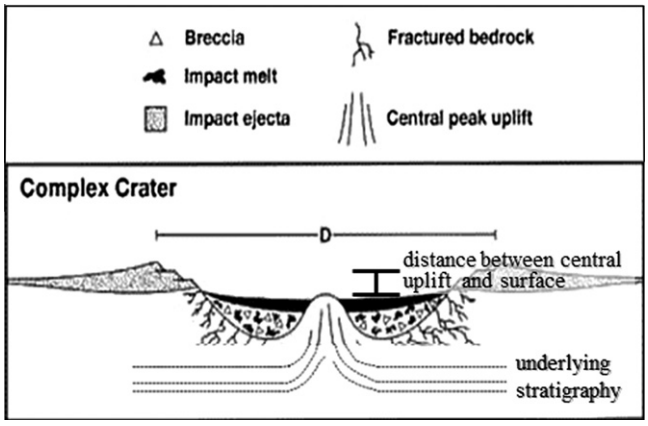

Fig. 7. Schematic of impact crater and underlying stratigraphy, proportions not to scale. Underlying stratigraphy is uplifted from depth in the crater's center while being fractured and tilted. "*D*" is the final crater diameter. Also shown is the depth of the central uplift (vertical distance between the central uplift and the surface). Diagram modified from Melosh (1989).

Table 3
Hesperian plains material with calculated volumes based on minimum LMB thickness (best approximation constrained by maximum depth exposures in craters, underlying topography, etc.).

Region	Area of plains (10^6 km^2)	Estimate of thickness of material (km)	Volume of material (10^6 km^3)
Thaumasia Planum	1.17	7.7	9.05
Syria/Sinai/Solis (SSS) Planums	1.25	13.9	17.36
Bosphorus Planum	0.29	4.6	1.36
Lunae Planum	1.16	5.1	5.89
Hesperia Planum	2.27	3.7	8.47
Syrtis Major Planum	1.68	7.7	12.86
Total			54.99

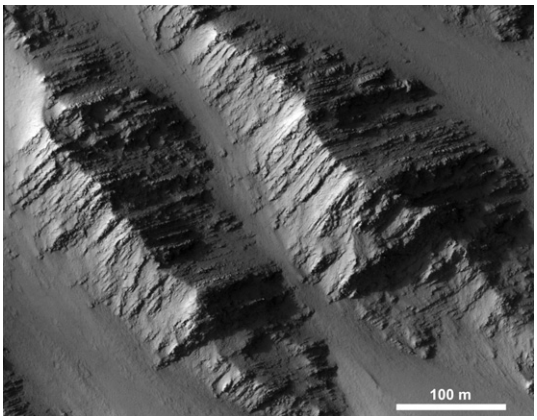

Fig. 8. Layers in a strongly tilted block on the northern scarp of Olympus Mons (23.2N, 223.6E). Based on the geologic setting, these layers are almost certainly composed of lavas and associated sediments. Note the similarities to LMB (Figs. 2 and 4) in terms of layer thicknesses and the mix of thin, resistant (high-standing) layers with less resistant (low-standing) layers. The Olympus Mons region is dust-covered so we could not see a relatively high albedo of the low-standing layers as in Fig. 4. Portion of HiRISE image ESP_027712_2035.

interpreted to be Hesperian-aged volcanic ashfall or airfall dust (Delt et al., 2010), apparently reworked in places as fluvial deposits (Weitz et al., 2010), but may also be present in the outer walls. As discussed in Section 3.1, LMB outcrops alternate between relatively higher-standing darker-toned layers and lighter-toned lower-standing layers with a measurable difference throughout LMB outcroppings (up to ~7.5 m). This height difference is likely related to the erosion resistance between two distinct lithologies represented in LMB and long-term exposure of these materials to surface processes. Similar to Large Igneous Province emplacement, these alternating layers and their relative competencies represent strong lithologies intercalated with less competent materials. Though the specific lithology is uncertain, both layers appear to be resistant enough to be preserved (in morphology and height) post-impact and over time. Tormanen et al. (2010) stated that morphology alone was a sufficient indicator in determining lithologic character of martian stratigraphy with high-resolution images. Their study found that layered material on the floors of Gale and Holden crater, interpreted as sedimentary, are distinguishable from layers emplaced by lava flows in Olympus and Pavonis Mons, Noctis Labyrinthus, Kasei Valles, and Sytris Major crater walls based on specific morphologic characteristics. This study used morphology not as a lithologic indicator, but as a way to identify sequence stratigraphy, which was then augmented with other analyses and geologic context. Morphologic similarities between layered material found on the Olympus Mons northern scarp (where they are strongly tilted like the LMB) and that of LMB is shown in Fig. 8.

4.2. Regional stratigraphy

The extent of layered volcanic material at depth can be further constrained by looking at SU of LMB along with two additional bedrock types from the Crater Exposed Bedrock database of Tornabene et al. (2010). These two additional bedrock textures are classified as Fractured Bedrock (FB), a relatively light-toned, fractured, and massive textured material that is possibly plutonic (also see Skok et al., 2010), and ancient MegaBreccia (MB), interpreted to be a re-sampling of crust previously brecciated from the period of heavy bombardment. Fig. 9 shows Bosphorus Planum having two distinct bedrock textures. An FB crater (−21°S, 306°E, D = 28.3 km) has a SU of 2.49 km and a pre-impact depth of 3.0 km. Within this mapped geologic unit, LMB ranges from 1.8 km to 4.6 km pre-impact depths. A stratigraphic boundary is

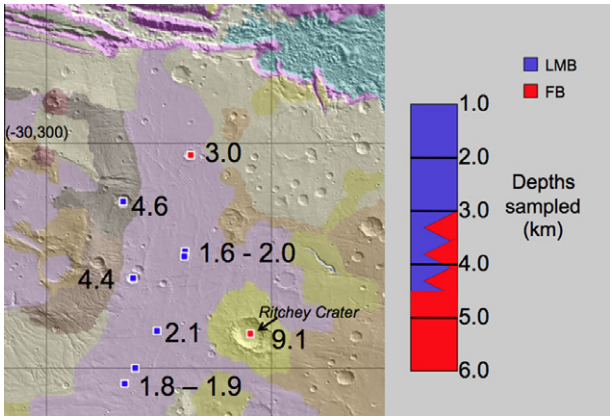

Fig. 9. Bosphorus Planum. JMARS data points overlain onto a geologic map (Skinner et al., 2006) noted with depth estimates (km) by each LMB or FB crater. Depths are also displayed in a vertical "stratigraphic column" on the right. Purple units are Hesperian ridged plains and dark brown is mapped as "mountainous material," both of which define the area of Bosphorus Planum in this study. (Right) Interfingering of the two bedrock textures likely occurs between depths of 3.0–4.6 km. Ritchey Crater is shown in the figure for reference; FB is found in Ritchey Crater with a depth estimate of 9.1 km, showing that the FB likely extends at depth, below LMB bedrock. (For interpretation of the references to color in this figure legend, the reader is referred to the web version of this article.)

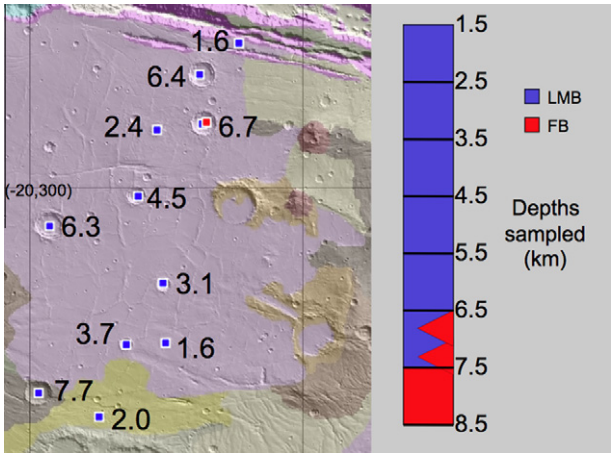

Fig. 10. Thaumasia Planum. Data points, showing depth estimates (km), overlain onto a geologic map (Skinner et al., 2006). Purple unit is Hesperian ridged plains. Right, a "stratigraphic column" displays depths of three bedrock types, where interfingering between LMB and FB likely occurs between depths of 6.7–7.7 km. (For interpretation of the references to color in this figure legend, the reader is referred to the web version of this article.)

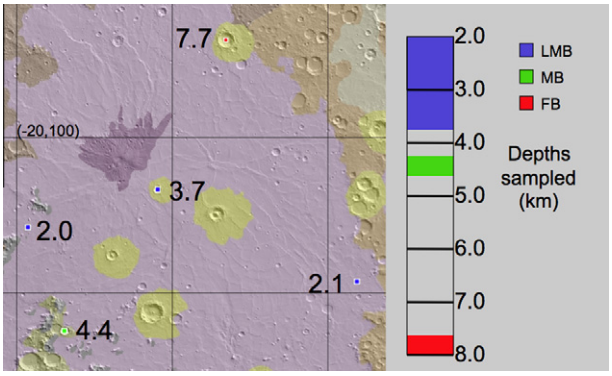

Fig. 11. Hesperia Planum. Data points, showing depth estimates (km), overlain onto a geologic map (Skinner et al., 2006). Purple unit is Hesperian ridged plains. Right, a "stratigraphic column" displays depths of three bedrock types; gray spaces indicates unknown stratigraphy. (For interpretation of the references to color in this figure legend, the reader is referred to the web version of this article.)

inferred to exist between these two bedrock textures at depth somewhere between 3.0 km and 4.6 km locally, if the LMB unit has a uniform thickness in this area. FB likely extends at depth in this region, based on larger craters sampling this material much more deeply. Ritchey Crater (−28°S, 309°E, D = 79.1 km) is the largest FB crater in the region, which samples FB at an estimated depth of 9.1 km below the surface. Ritchey Crater and the aforementioned unnamed FB crater in this region straddle a contact between the Hesperian ridged plains and Noachian plateau (Npl1 and Npl2, respectively) as mapped by Skinner et al. (2006). We infer that the layered materials that correlate with the Hesperian ridged plains unit likely thins out as the boundary between these two units are approached. As such, the unnamed crater and Ritchey Crater may have sampled layered materials but they were likely too shallow to be exposed within their central uplifts, or we cannot recognize them in present-day exposures. Overall, these observations and estimates indicate a gross regional stratigraphy for Bosphorus Planum that consists of massive-textured bedrock, possibly plutonic, at greater stratigraphic depths overlain by layered bedrock, suggested here as layered volcanic material, and a thin regolith covering.

Fig. 10 shows the Crater Exposed Bedrock in Thaumasia Planum, which is dominated by the occurrence of LMB craters, having one crater that shows both LMB and FB textures within a single crater central uplift. The crater exhumed these materials from an estimated depth of 6.7 km and uniquely reveals a stratigraphic boundary between these two materials at a single location. FB is found no shallower than 6.7 km, but only occurs in the aforementioned crater, whereas LMB ranges from 1.6 km to 7.7 km throughout Thaumasia Planum. As a possible comparison to this material, Edwards et al., 2008 analyzed the mineral composition of walls in Valles Marineris (Ganges and Eos Chasma), and found olivine-enriched signatures were typically found ~3.5–4 km below the rim. They also concluded that this material was more consolidated than aeolian sediments and likely of flood lava origin, consistent with our data for circum-Valles Marineris LMB. FB materials likely represents deeper, possibly plutonic material as previously suggested (Tornabene et al., 2010; Skok et al., 2010; Caudill et al., 2011; Flahaut et al., 2012). As observed in Bosphorous Planum, the stratigraphy of Thaumasia Planum, based on Crater Exposed Bedrock, consists of deep-seated FB materials overlain by LMB and a thin regolith.

4.3. Regional LMB layers and unit thickness

LMB material at depth can further be examined by focusing on the extent of the material (thickness of the unit) as well as the number of layers, possibly lava cooling units, which may exist in a given regional LMB unit. Crater scaling gives an estimate of the section uplift (SU), and with the assumption that the LMB brought from depth are consistent with the surface materials, the LMB material likely extends to the surface. This assumption that the surface materials are the same type of material as LMB is based on surface morphology (lava plains, wrinkle ridges) of mapped Hesperian plains material and the high correlation of this surface material with pit peak features in LMB central uplifts, which may speak to the layer characteristics at depth. Whitehead et al. (2010) have interpreted Hesperian lava plains target strength as correlating with that of coherent basalt, which is much higher than that of sedimentary targets, and concluded that peak pits have a statistically significant higher occurrence on such lava-dominated targets consequent of their target yield strength. Seventy-five percent of the 41 LMB craters reported in this study have peak pit morphology, while 20% have central peaks. Two LMB craters were not given an assigned central uplift morphology due to the apparent erosion of the crater as evidenced by the collapsed or eroded crater rims and/or infilling of material. The densest cluster of LMB craters of any region occurs in Thaumasia Planum, which has the highest percentage of peak pit craters; 90% of LMB craters in this region have peak pit morphology. As expressed in Figs. 9–11, the LMB material in these regions appear to be the material at depth that is closest to the surface. This stratigraphic placement of the LMB material was coupled with the assumption that the material extends from the depths calculated to the surface to assess the unit thickness of the LMB material (Table 2).

Average layer thickness within LMB outcroppings was measured (Table 1) and then paired with LMB unit thickness (Table 2) to estimate the possible number of cooling units that may exist within a given region ("minimum regional flood lava thickness," Table 4). Estimating the number of cooling units allowed us to assess if the number of possible cooling units supported evidence for intermittent effusive flood lavas throughout the Hesperian Era. Terrestrial basaltic flows in Large Igneous Provinces produce effusive flow sheets, where single cooling units are each flows or sets of flows emplaced closely in time. Keszthelyi et al. (2006) assessed martian flood lavas as having intermittent effusion rates of 10^6 m^3 s^{-1}, consistent with effusion rates estimated for the terrestrial Columbia River Flood Basalt Group where flows covered tens of thousands of kilometers (Swanson et al., 1975). Based on the

Table 4
Minimum flood lava thicknesses derived from section uplift estimates (SU) of crater central peak LMB bedrock exposures. Average layer thickness within these units is determined by extraction of spatial data along individual layers, fitting adjacent planes for orientation and distance determination. The observed (minimum) thickness lava stack per region, assuming average layer thickness is consistent throughout the unit, yields the possible number of cooling units.

Region	Minimum regional flood lava thickness (km)	Average layer thickness (m)	Possible number of cooling units
Thaumasia Planum	7.7	17.8	433
Syria/Siani/Solis Planums	13.9	6.0	2317
Bosphorus Planum	4.6	2.8	1643
Acidalia Planum	3.2	19.5	164
Lunae Planum	5.1	10.3	495
Kasei Valles	2.4	16.4	146

estimated LMB unit thickness in the Syria/Sinai/Solis Planums region, the possible number of cooling units could conceivably exceed 2300. This suggests that a large number of eruptive episodes may have occurred to form the stack of flood lavas and interbedded sediments expressed in LMB craters. Gillmann et al. (2011) studied past martian climate and volatiles in the atmosphere over time as a result of volcanism, assumed to be continuous over time, and stated that if volcanic eruptions actually occur episodically (which they do), model results may differ. Head and Wilson (2011) investigated Hesperian volcanism and found that this period was a time of "peak volcanic flux" having extensive, voluminous, and low viscosity events. Furthermore, Head and Wilson (2011) stated that this would have a significant effect on released volatiles and global climate. Data presented here may be useful to refine models of the ancient martian climate.

A major limitation for LMB thickness estimates is the availability of large craters with well-exposed bedrock, however, the ranges reported here allow a first-order assessment of the extent of these materials. LMB thickness estimates as well as the thickness of the individual layers (Table 4) are consistent with terrestrial flood basalt provinces on Earth. Such Large Igneous Provinces include the Ghats region of the Deccan Traps, where the flood lavas are estimated to be 3 km thick (Sheth, 1999) and the main Deccan Province typically has individual flow units 20–30 m thick with 1–10 m thickness dominating some regions (Jerram and Widdowson, 2004). Larsen and Tegner (2005) calculated thickness of volcanic overburden of the East Greenland flood basalts, where between 2.4 ± 1.5 and 10 ± 4.4 km estimated unit thicknesses were based on pressure–temperature estimates from fluid inclusions in granophyres differentiated from olivine tholeiitic magma. The ~5 km thick Emeishan flood basalts in SW China have been documented to consist of 12 separate units, ranging in thickness between 10 and 140 m (Qi and Zhou, 2007). One other terrestrial example of flood basalt dimensions similar to those we estimate for Mars include the southern Namibia Kalkrand Formation, which also consist of sheet-like lava flows with sediments interleaved, has individual lava flows ranging from 0.5 to 12 m with upper-most flow sequence of inflated lava flow approaching 30 m (Stollhofen et al., 1999). Jerram and Widdowson (2004) also note that the aforementioned Western Ghats formation individual flows follow complex thinning and thickening patterns, separated by eroding layers that correspond to the periodicity of eruptions. These observations highlight that our assumption that individual layer thickness continues throughout the stratigraphic unit of the flood lavas of a given region, which allows for our estimates of possible number of cooling units by region, is simplistic. As noted by Peterson et al. (1994) and Stollhofen et al. (1999), known deformational features occur in flood lava units; wrinkle ridge formation begins as flat lava flows then bulges the crust, resulting in a local increase in the thickness of the flow. Such features show that flood basalt emplacement is a complex process where the thickness of stratigraphy is variable given any singular episode. However, the scale of the number of cooling units, as well as the thickness of the entirety of the units described here is consistent with the terrestrial analogs provide useful order-of-magnitude estimates of past volcanic activity during the Hesperian period on Mars.

4.4. Volume estimates and atmospheric implications

Estimating volumes of extruded flood lavas over the history of Mars is essential to learning about the past geology and atmosphere, but presents quite a challenge considering the paucity of stratigraphic exposures on Mars to study the depths of flood lavas over time. Remote-sensing methods for determining volumes of extrusive volcanics on Mars have been described (De Hon, 1979). Greeley and Schneid (1991) used partially buried craters whose rims were still visible, and an original crater depth-diameter ratio was calculated for comparison to determine the thickness of the invading lavas (De Hon, 1979). It was assumed that this method gives minimum values for thicknesses because the craters could rest on older volcanic materials. However, the authors noted that this could also give an overestimate of lava thickness if some craters were infilled by other post-impact materials prior to flooding by lava, as is the case for many large Noachian craters. De Hon (1982) discusses other limitations of this method on Mars. Greeley and Schneid (1991) were able to determine volume estimates for lavas during each epoch of Mars (Table 5), with the total martian history, excluding the unconstrained Early Noachian, accumulating $\sim 68.8 \times 10^6$ km^3. This same technique was also used by Ivanov et al. (2005) to estimate the volume of lavas in Hesperia Planum, where craters where found to be buried by several hundred meters, with an estimated total volume for the unit of ~ 0.4–0.7×10^6 km^3. Craddock and Greeley (2009) and Gillmann et al. (2011) state that techniques have not changed sufficiently to update estimates of volumes of extrusives, as the Greeley and Schneid estimates have been the basis for models approximating outgassing as it pertains to past martian atmospheres.

Here, we seek to update minimum values for extrusive flows and pyroclastics for this period of voluminous volcanism, namely late-Noachian through the Hesperian Epoch with the data collected from our sample population of LMB craters. Table 6 shows previous estimates for extrusives by Greeley and Schneid (1991) along with figures updated to include our estimates for late Noachian/Hesperian extrusive flood lavas. In contrast to the previous methods, we use the section uplift of craters that expose pre-impact bedrock and thus provide information about the subsurface. This study's calculated volumes for LMB (Table 3) therefore produce an alternate estimate for extrusive minimums, raising the estimate during this period to 55×10^6 km^3. This is consistent with Greeley

Table 5
Extrusive volumes of volcanic material on Mars over time (Greeley and Schneid, 1991).

Epoch	Volume of plains (10^6 km^3)	Volume of edifices (10^6 km^3)	Extruded volume (10^6 km^3)
Late Amazonian			
Middle Amazonian	1.42	7.07	8.49
Early Amazonian	3.61	12.15	15.76
Late Hesperian	4.54	11.09	15.63
Early Hesperian	10.83	6.82	17.65
Late Noachian	4.31	3.46	7.77
Middle Noachian	1.39	0	1.39
Early Noachian	?	?	?
Total	26.43	42.37	68.8

Table 6
Extrusive volumes by epoch as estimated by Greeley and Schneid (1991), as well as this study's updated volume estimate for the Hesperian/Noachian Epochs. This study's extrusive total reflects estimates for extrusives from Greeley and Schneid (1991) for the Amazonian Epoch and are updated with our Hesperian/Noachian extrusive estimates.

Epoch	Greeley and Schneid, 1991 (10^6 km^3)	This study (10^6 km^3)
Amazonian	26.36	(Assume 26.36)
Hesperian/Noachian	42.44	54.99
Total	68.80	81.35

and Schneid (1991) who submitted that their figures may have been underestimates. Our values may also be an underestimate of total Hesperian extrusives because most of the craters do not expose the deepest layers. At 55×10^6 km^3, our estimates for this time period increase total extrusives by 22.8% for the volcanic history of Mars (see Table 6).

The estimates of Craddock and Greeley (2009) can be increased 23% based on the results of this paper, although greater uncertainty still exists in the released volatile content of the magma (e.g., McSween et al., 2001; Stanley et al., 2011; Grott et al., 2011). Greenhouse warming may have been significant not only from CO_2, but also volcanic sulfur (Johnson et al., 2008). Water release to the environment was directly exsolved from the magma, also, ground ice was disrupted by the volcanism causing enhanced ice sublimation associated with greenhouse warming. In summary, the late Noachian–Hesperian volcanism may have played a major role in producing the extensive sulfate deposits (Squyres, 2004; Gendrin et al., 2005; many others) and Hesperian fluvial activity and aqueous alteration (e.g., Weitz et al., 2010; Le Deit et al., 2010; Grant and Wilson, 2011).

5. Summary and conclusions

Based on a previous survey of over 900 HiRISE observations, a dataset of bedrock outcroppings identified 41 crater central uplifts as having distinctive Layered MegaBlocks (LMB). We interpret the LMB as being emplaced primarily by flood volcanism during the Hesperian Epoch (and perhaps later Noachian for deep layers). This is based on the high geographic correlation of LMB craters with Hesperian ridged volcanic plains, their similarity in layer thickness and total extent to sequences of volcanic materials in large volcanic provinces on Earth (Qi and Zhou, 2007; Stollhofen et al., 1999; Larsen and Tegner, 2005), and mineralogic evidence from Quantin et al. (2011). As these bedrock outcroppings are uplifted and tilted consequent of crater formation the layer orientations become more vertical and are visible in high-resolution images taken from orbit, as opposed to layers exposed in canyons and craters walls which are nearly horizontal. This makes layered central uplifts prime for analysis of layered bedrock from orbit. Morphometric analysis of LMB indicates that they have what we interpret to be weaker, less erosion resistant layers interleaved with stronger, more competent layers. Analyses of these features show that this material is morphologically analogous to layered sequences seen in terrestrial Large Igneous Provinces.

Section uplift estimates of circum-Valles Marineris LMB correlate to depths of Valles Marineris wall layering, where sequences of strong layers and relatively weak layers are interpreted to be emplaced by episodic intercalated flood lavas and pyroclastics and other sediments. The differences in tonality of the layers represented by LMB correlate with layers outcropping in Valles Marineris, though the orientations of the outcrops at the two settings and the geologic history post-emplacement make them difficult to compare visually using orbital data.

Depth estimates allow for minimum upper and lower bounds of subsurface layers when analyzed with additional bedrock textures and their depths. Volume estimates of material interpreted as extensive flood lava sequences are then estimable. Section uplift estimates based on diameters of LMB craters, paired with individual layer thickness measurements, show that hundreds of cooling units may exist below the surface in these regions. This supports highly episodic and punctuated volcanic activity throughout the Hesperian and possibly the late Noachian periods consistent with Head and Wilson (2011). If this material indeed represents late Noachian and Hesperian extrusives, our volume estimates indicate a 22.8% increase when compared with previous estimates, which has implications for modeling past climates on Mars.

References

Beyer, R., McEwen, A., 2005. Layering stratigraphy of eastern Coprates and northern Capri Chasmata, Mars. Icarus 179, 1–23.
Bray, V.J. et al., 2012. Ganymede crater dimensions – Implications for peak and pit formation and development. Icarus 217, 115–129.
Bryan, S. et al., 2010. The largest volcanic eruptions on Earth. Earth-Sci. Rev. 102, 207–229.
Byrne, S., Ivanov, A., 2004. Internal structure of the martian south polar layered deposits. J. Geophys. Res. 19, E11001.
Carr, M.H., Head, J.W., 2010. Geologic history of Mars. Earth Planet. Sci. Lett. 294, 3–4.
Caudill, C. et al., 2011. Crater-exposed intact stratigraphy blocks and volcanogenic origin. Lunar Planet. Sci. 42, 2393.
Christensen, P.R. et al., 2004. The Thermal Emission Imaging System (THEMIS) for the Mars 2001 Odyssey mission. Space Sci. Rev. 110 (1), 85–130.
Christensen, P.R. et al., 2009. JMARS – A planetary GIS. AGU 2009, #IN22A-06.
Cintala, Grieve, 1993. Differential scaling: Implications for central structures in large lunar craters. Lunar Planet. Sci. 24, 291.
Craddock, R., Greeley, R., 2009. Minimum estimates for the amount and timing of gases released into the martian atmosphere from volcanic eruptions. Icarus 204, 512–526.
Craddock, R.A. et al., 1997. Crater morphometry and modification in the Sinus Sabaeus and Margaritifer Sinus regions of Mars. J. Geophys. Res. (Planets) 102, 13321–13340.
De Hon, R.A., 1979. Thickness of the western mare basalts. Proc. Lunar Sci. Conf. 10, 2935–2955.
De Hon, R.A., 1982. Mars volcanic materials: Preliminary thickness estimates in the eastern Tharsis region. J. Geophys. Res. 87, 9821–9828.
Delt, L. et al., 2010. Morphology, stratigraphy, and mineralogical composition of a layered formation covering the plateaus around Valles Marineris, Mars: Implications for its geological history. Icarus 208, 684–703.
Edwards, C.S. et al., 2008. Evidence for extensive olivine-rich basalt bedrock outcrops in Ganges and Eos Chasmas, Mars. J. Geophys. Res. 113, 3091.
Edwards, C.S. et al., 2009. Global distribution of bedrock exposures on Mars using THEMIS high-resolution thermal inertia. J. Geophys. Res. 114, E11.
Ernst, R. et al., 2004. Frontiers in Large Igneous Province research. Lithos 79, 271–297.
Flahaut, J. et al., 2010. Phyllosillicates and low calcium pyroxene-rich Noachian crust exposures in the walls of Valles Marineris, Mars. Lunar Planet. Sci. 41, 1524.
Flahaut, J. et al., 2011. Dikes of distinct composition intruded into Noachian-aged crust exposed in the walls of Valles Marineris. Geophys. Res. Lett. 38, L15202.
Flahaut, J. et al., 2012. Pristine Noachian crust and key geologic transitions in the lower walls of Valles Marineris: Insights into early igneous processes on Mars. Icarus. http://dx.doi.org/10.1016/j.icarus.2011.12.027.
French, B.M., 1998. Traces of Catastrophe; A of Shock Metamorphic Effects in Terrestrial Meteorite Impact Structures. Contribution No. 945. Lunar and Planetary Institute, Houston.
Garvin, J., Frawley, J., 1998. Geometric properties of martian impact craters: Preliminary results from the Mars Orbiter Laser Altimeter. Geophys. Res. Lett. 25, GL900177.
Geissler, P.E. et al., 1990. Dark materials in Valles Marineris: Indications of the style of volcanism and magmatism on Mars. J. Geophys. Res. 95, 14399–14413.
Gendrin, A. et al., 2005. Sulfates in martian layered terrains: The OMEGA/Mars express view. Science 307, 1587–1591.
Gillmann, C. et al., 2011. Volatiles in the atmosphere of Mars: The effects of volcanism and escape constrained by isotopic data. Earth Planet. Sci. Lett. 303, 299–309.
Golombek, M.P., Anderson, F.S., Zuber, M.T., 2001. Martian wrinkle ridge topography: evidence for subsurface faults from MOLA. J. Geophys. Res. Planet. 106, 23811–23821.
Grant, J.A., Wilson, S.A., 2011. Late alluvial fan formation in southern Margaritifer Terra, Mars. Geophys. Res. Lett. 38, L08201.
Greeley, R., Guest, J., 1987. USGS Map I-1802-B.
Greeley, R., Schneid, B., 1991. Magma generation on Mars: Amounts, rates, and comparisons with Earth, Moon, and Venus. Science 254, 996–998.

Greeley, R., Spudis, P., 1981. Volcanism on Mars. Rev. Geophys. Space Phys. 19, 13–41.
Grieve, R., Pilkington, M., 1996. The signature of terrestrial impacts. AGSO J. Aust. Geol. Geophys. 16, 399–420.
Grieve, R., Therriault, A.M., 2004. Observations at terrestrial impact structures: Their utility in constraining crater formation. Meteorit. Planet. Sci. 39, 199–216.
Grieve, R. et al., 1981. Constraints on the formation of ring impact structures based on terrestrial data. Proc. Lunar Sci. Conf. 12A, 37–57.
Grott, M. et al., 2011. Volcanic outgassing of CO_2 and H_2O on Mars. Earth Planet. Sci. Lett. 308, 391–400.
Hales, T. et al., 2005. A lithospheric instability origin for Columbia River Flood Basalts and Wallowa Mountains uplift in northeast Oregon. Nature 438, 842–845.
Head, J.W., Wilson, L., 2011. The Noachian–Hesperian transition on Mars: Geological evidence for a punctuated phase of global volcanism as a key driver in climate and atmospheric evolution. Lunar Planet. Sci. 42, 1214.
Ivanov, B.A. et al., 2005. Major episodes of the hydrologic history in the region of Hesperia Planum, Mars. J. Geophys. Res. 110, E12S21.
Jaeger, W.L. et al., 2010. Emplacement of the youngest flood lava on Mars: A short, turbulent story. Icarus 205, 230–243.
Jerram, D., Widdowson, M., 2004. The anatomy of Continental Flood Basalt Provinces: Geological constraints on the processes and products of flood volcanism. Lithos 79, 385–405.
Johnson, S. et al., 2008. Longevity of atmospheric SO_2 on early Mars. Lunar Planet. Sci. 39, 2090.
Keszthelyi, L., McEwen, A., 2007. Comparison of flood lavas on Earth and Mars. In: Chapman, M. (Ed.), The Geology of Mars: Evidence from Earth Based Analogues. United States Geological Survey, Arizona, pp. 126–150.
Keszthelyi, L. et al., 2006. Flood lavas on Earth, Io, and Mars. J. Geol. Soc. 163, 253–264.
Keszthelyi, L. et al., 2008. High Resolution Imaging Science Experiment (HiRISE) images of volcanic terrains from the first 6 months of the Mars Reconnaissance Orbiter Primary Science Phase. J. Geophys. Res. 113, CiteID E04005.
Kirk, R.L. et al., 2008. Ultrahigh resolution topographic mapping of Mars with MRO HiRISE stereo images: Meter-scale slopes of candidate Phoenix landing sites. J. Geophys. Res. 113, CiteID E00A24. http://dx.doi.org/10.1029/2007JE003000.
Komor, S. et al., 1988. Fluid-inclusion evidence for impact heating at the Siljan Ring, Sweden. Geology 16, 711–715.
Larsen, R., Tegner, C., 2005. Pressure conditions for the solidification of the Skaergaard intrusion: Eruption of East Greenland flood basalts in less than 300,000 years. Lithos 92, 181–197.
Larson, D. et al., 2009. Postimpact Alteration of Sedimentary Breccias in the ICDP_USGS Eyreville A and B Cores with Comparison to the Cape Charles Core, Chesapeake Bay Impact Structure, Virginia, USA. The Geological Society of America, Special Paper 458.
Le Deit, L. et al., 2010. Morphology, stratigraphy, and mineralogical composition of a layered formation covering the plateaus around Valles Marineris, Mars: Implications for its geological history. Icarus 208, 684–703.
Malin, M.C., Edgett, K.S., 2001. Mars Global Surveyor Mars Orbital Camera: Interplanetary cruise through primary mission. J. Geophys. Res. 106, 23429–23570.
Malin, M.C. et al., 2007. Context Camera Investigation on board the Mars Reconnaissance Orbiter. J. Geophys. Res. 112, E05S04.
McEwen, A. et al., 1999. Voluminous volcanism on early Mars revealed in Valles Marineris. Nature 397, 584–586.
McEwen, A.S. et al., 2007. Mars Reconnaissance Orbiter's High Resolution Imaging Science Experiment (HiRISE). J. Geophys. Res. 112, E05S02.
McEwen, A.S. et al., 2010. The High Resolution Imaging Science Experiment (HiRISE) during MRO's Primary Science Phase (PSP). Icarus 205, 2–37.
McSween, H.Y. et al., 2001. Geochemical evidence for magmatic water within Mars from pyroxenes in the Shergotty meteorite. Nature 409, 487–490.
Melosh, H.J., 1989. Impact Cratering: A Geologic Process. Oxford Univ. Press, New York, pp. 245.
Nichols, R.L., 1936. Flow units in basalt. J. Geol. 44, 617–630.
O'Keefe, J.D., Ahrens, T.J., 1999. Complex craters: Relationship of stratigraphy and rings to impact conditions. J. Geophys. Res. 104, 27091–27104.
Peterson, D.W., Holcomb, R.T., Tilling, R.I., Christiansen, R.L., 1994. Development of lava tubes in the light of observations at Mauna Ulu, Kilauea Volcano, Hawaii. Bull. Volcanol. 56, 343–360.
Pike, R.J., 1980. Control of crater morphology by gravity and target type: Mars, Earth, and Moon. Proc. Lunar Sci. Conf. 11, 2159–2189.
Pilkington, M., Grieve, R., 1992. The geophysical signature of terrestrial impact craters. Rev. Geophys. 30, 161–181.
Qi, L., Zhou, M., 2007. Platinum-group elements and Sr–Nd–Os isotopic geochemistry of Permian Emeishan flood basalts in Guizhou Province, SW China. Chem. Geol. 248, 83–103.
Quantin, C. et al., 2011. Composition and structures of the subsurface in the vicinity of Valles Marineris as revealed by central uplifts of impact craters. Lunar Planet. Sci. 42, #2342.
Riedel, S.P., 2005. A lava flow without a source: The Cohassett flow and its compositional components, Sentinel Bluffs Member, Columbia River Basalt Group. J. Geol. 113, 1–21.
Schultz, R.A., 2002. Stability of rock slopes in Valles Marineris, Mars. Geophys. Res. Lett. 29, GL015728.
Scott, D.H., Tanaka, K.L., 1986. USGS Map I-1802-A.
Self, S., Thordarson, T., Keszthelyi, L.P., 1997. Emplacement of Continental Flood Basalt Lava Flows, in Large igneous provinces; continental, oceanic, and planetary flood volcanism. In: Mahoney, J.J., Coffin, M.F. (Eds.), vol. 100. American Geophysical Union, Washington, DC, pp. 381–410.
Sheth, H.C., 1999. Flood basalts and large provinces from deep mantle plumes: Fact, fiction, and fallacy. Tectonophysics 311, 1–29.
Skinner, J. et al., 2006. Digital renovation of the atlas of Mars 1:15,000,000-scale global geologic series maps. Lunar Planet. Sci. 37, 2331.
Skok, J. et al., 2010. Crystalline igneous crust of Mars: New insights form the southern highlands. Lunar Planet. Sci. 41, 1926.
Smith, D. et al., 2001. Mars Orbiter Laser Altimeter: Experiment summary after the first year of global mapping of Mars. J. Geophys. Res. 106, 689–722.
Squyres, S.W., 2004. Aqueous processes on Mars: Results from the Mars Exploration Rover Mission. AGU (Fall Meet.), P13B-01.
Stanley, B. et al., 2011. CO_2 solubility in martian basalts and martian atmospheric evolution. Geochim. Cosmochim. Acta 75, 5987–6003.
Stollhofen, H. et al., 1999. Tectonic and volcanic controls on Early Jurassic rift-valley lake deposition during emplacement of Karoo flood basalts, southern Namibia. Palaeogeogr., Palaeoclimatol., Palaeoecol. 140, 185–215.
Swanson, D. et al., 1975. Linear vent systems and estimated rates of eruption for the Yakima basalt on the Columbia Plateau. Am. J. Sci. 275, 877–905.
Tanaka, K., 1986. The stratigraphy of Mars. J. Geophys. Res. 91, http://dx.doi.org/10.1029/0JGREA000091000B1300E139000001. ISSN: 0148-0227.
Tompkins, S., Pieters, C.M., 1999. Mineralogy of the lunar crust: Results from Clementine. Meterorit. Planet. Sci. 34, 25–41.
Tormanen, T. et al., 2010. End-member morphologies of volcanic and sedimentary layered rocks on Mars from the high-resolution images. Lunar Planet. Sci. 41, 1310.
Tornabene, L.L. et al., 2010. A Crater Exposed Bedrock database for Mars with applications for determining the composition and structure of the upper crust. Lunar Planet. Sci. 41, 1737.
Weitz, C. et al., 2010. Mars Reconnaissance Orbiter observations of light-toned layered deposits and associated fluvial landforms on the plateaus adjacent to Valles Marineris. Icarus 205, 73–102.
Whitehead, J. et al., 2010. The effects of crater degradation and target differences on the morphologies of martian complex craters. Spec. Pap. Geol. Soc. Am. 465, 67–80.
Williams, J.P. et al., 2003. Layering in the wall rock of Valles Marineris: Intrusive and extrusive magmatism. Geophys. Res. Lett. 30, CiteID 1623. http://dx.doi.org/10.1029/2003GL017662.
Wilson, L., Head, J., 1994. Mars: Review and analysis of volcanic eruption theory and relationships to observed landforms. Rev. Geophys. 32, 221–263.
Wood, C. et al., 1978. Interior morphology of fresh martian craters: The effects of target characteristics. Proc. Lunar Sci. Conf. 9, 3691–3709.